Nano Energy 73 (2020) 104804

Contents lists available at ScienceDirect

Nano Energy

journal homepage: http://www.elsevier.com/locate/nanoen

Ultra-efficient polymer binder for silicon anode in high-capacity lithium-ion batteries

Shilun Gao [a], Feiyuan Sun [a], Alexander Brady [b], Yiyang Pan [a], Andrew Erwin [b,c], Dandan Yang [d], Vladimir Tsukruk [c], Andrew G. Stack [b], Tomonori Saito [b], Huabin Yang [a,e,*], Peng-Fei Cao [b,**]

[a] Institute of New Energy Material Chemistry, School of Materials Science and Engineering, Nankai University, Tianjin, 300350, China
[b] Chemical Sciences Division, Oak Ridge National Laboratory, Oak Ridge, TN, 37830, United States
[c] School of Materials Science and Engineering, Georgia Tech, Atlanta, GA, 30332, United States
[d] Experimental Teaching Center of Materials Science, School of Materials Science and Engineering, Nankai University, Tianjin, 300350, China
[e] Tianjin Key Laboratory of Metal and Molecular Based Material Chemistry, School of Materials Science and Engineering, Nankai University, Tianjin, 300350, China

ARTICLE INFO

Keywords:
Polymer binder
Silicon anode
Li-ion batteries
Polyimine

ABSTRACT

As a highly promising anode material for high-capacity lithium-ion batteries (LIBs), the low electronic conductivity and large volume variation of silicon (Si) make the slurry-coating Si based electrode requiring high content of "inert" materials and suffering rapid capacity fading. Herein, a polyimine, synthesized *via* one-step condensation reaction, has been demonstrated as an ultra-efficient polymer binder that can resolve the above issues. The polyimine binder containing Si electrode delivers superior electrochemical performance: a delithiation specific capacity of 804.4 mAh g^{-1} with capacity retention of 82.4% after 1000 cycles at the current density of 2 A g^{-1}. The high efficiency of polyimine binder for Si electrode has also been demonstrated with ultrahigh weight ratio of "active" material to "inert" material ($R_{A/I}$). The electrode with 95 wt% of Si (95Si/Polyimine, $R_{A/I} = 19$) reveals a reversible delithiation capacity of 2114 mAh g^{-1} (capacity retention ~ 80.4%) over 200 cycles at the current density of 400 mA g^{-1}. Even at the high current density of 2 A g^{-1}, a delithiation capacity of 1087.8 mAh g^{-1} after 500 cycles can be obtained. Molecular simulations and atomic force microscopy (AFM) indentation are utilized to investigate the ultra-efficiency of polyimine binder. With simple manufacturing process and ultra-efficient binder performance, the designed polyimine binder will be definitely meaningful in achieving low-cost and high-capacity LIBs with prolonged cycle life.

1. Introduction

Lithium-ion batteries (LIBs) have been immensely used in portable electronic devices, electric vehicles and smart grids [1–5], while the widely used anode material, i.e. graphite, only shows a theoretical specific capacity of 372 mAh g^{-1} [6,7]. Silicon (Si) has demonstrated great potential as the anode material in LIBs due to its ultra-high theoretical specific capacity (3579 mAh g^{-1}), moderate operating voltage (<0.5 V vs Li/Li^+) and abundance in the earth's crust [8–14]. However, the significant volume variation (~300%) of Si during the repeated lithiation/delithiation process leads to the pulverization of Si, an unstable solid electrolyte interphase (SEI) layer and the isolation of active materials from the conductive network, resulting in the rapid capacity fading of Si electrodes [15–21]. Many efforts have been devoted to address the aforementioned problems, which can be mainly divided into two categories: structural regulation of active materials and development of efficient "inert" materials, i.e., polymer binders. Although Si electrodes consisting of defined nanostructures such as nanowires, nanorods, nanosheets, nanotubes, hollow/porous sphere, thin film and coating with other materials, exhibit significantly improved electrochemical performance, this approach always suffers from complicated fabrication process, expensive devices and difficulties in mass production [22–29]. Developing efficient polymer binders is an alternative approach with great potential in practical applications considering its relatively low-cost, facile and scalable slurry-coating techniques [30–35].

There are mainly two categories of binder materials: non-conductive polymers and conductive polymers [36,37]. For the non-conductive binders, a conventional polymer polyvinylidene fluoride (PVDF) fails in Si electrodes due to its weak van der Waals force with Si surface [38].

* Corresponding author. Institute of New Energy Material Chemistry, School of Materials Science and Engineering, Nankai University, Tianjin, 300350, China.
** Corresponding author. Chemical Sciences Division, Oak Ridge National Laboratory, Oak Ridge, TN, 37830, United States.
E-mail addresses: hb_yang@nankai.edu.cn (H. Yang), caop@ornl.gov (P.-F. Cao).

https://doi.org/10.1016/j.nanoen.2020.104804
Received 4 December 2019; Received in revised form 27 March 2020; Accepted 3 April 2020
Available online 10 April 2020

Therefore, a large number of polymeric materials with enhanced adhesion force with Si have been developed, such as sodium carboxymethyl cellulose (CMC) [39], poly(acrylic acid) (PAA) [40], alginate (Alg) [9] and modified natural polysaccharide [41]. Some other strategies including the use of self-healing polymers [42], polyrotaxanes with sliding ring motions [43], polymers with ionic conducting groups [44] and in-situ cross-linked polymer networks [45], have also been reported useful in improving the cycling performance of Si electrodes. Recently, we also reported a polymer binder with optimized adhesion functionality and mechanical robustness *via* tuning both grafting density of adhesion groups and degree of crosslinking [46]. However, most of these Si based electrodes require high content of inert materials, i.e., low weight ratio of "active" materials to "inert" material ($R_{A/I}$), usually 20–40 wt% of polymer binder (+conductive additives, $R_{A/I} \sim 4$–3/2) for Si electrode *vs* 5 wt% for graphite based electrode ($R_{A/I} \sim 19$), and high content of "inert" materials leads to increased cost and lower energy efficiency of obtained Si electrode [47–49].

Till now, developing the efficient polymer binder enabling the slurry-coating Si electrodes with a long cycle life and high $R_{A/I}$ have rarely been reported, and such achievement is especially meaningful in practical application of high energy-density LIBs. Conductive polymers are more promising due to their multifunctional role as both the binder material and conducting component [50–54]. Using an in-situ secondary doping treatment of the poly(3,4-ethylenedioxythiophene):poly (styrenesulfonate) (PEDOT:PSS) with formic acid, Higgins et al. studied the Si-electrodes with a wide range of Si contents (70–95 wt%), wherein poor electrochemical performance was observed for the electrodes with Si contents higher than 80 wt% ($R_{A/I} > 4$) [50]. Liu and co-workers also introduced the polymer binder poly(1-pyrenemethyl methacrylate-co-methacrylic acid) that allowed for the design of electrodes containing 90 wt% of Si. Although relatively high specific capacity was obtained, the capacity retention was only 74.6% after 100 cycles based on the 5th cycle [52]. Liang and coworkers prepared a conductive polymer binder by partial carbonization of natural polymers, and enhanced electrochemical performance can be obtained even at a high Si content (90 wt%), while the capacity retention needs to further optimization (a discharge capacity of 774 mAh g^{-1} after 300 cycles at 0.33 C) [55].

Herein, we present the design of an ultra-efficient conductive polymer binder, polyimine, allowing a slurry-coating Si electrode with high $R_{A/I}$ value (up to 19) and long cycle life (500–1000 cycles). The obtained electrode (70Si/Polyimine, the weight ratio of Si in the electrode is 70 wt%) delivers the highly stable cycling performance with capacity retention of 82.4% after 1000 cycles (delithiation capacity of 804.4 mAh g^{-1} at C/2). The electrode with ultra-low "inert" content (95Si/Polyimine, $R_{A/I} = 19$) can still maintain excellent cycling stability (capacity retention of 80.4% after 200 cycles based on the 4th cycle, C/10), outstanding rate capability (~1913 mAh g^{-1} at C/4 and ~1413 mAh g^{-1} at C/2) and superior long-term cycling performance (delithiation capacity of 1087.8 mAh g^{-1} after 500 cycles at C/2). Although the prepared polymer binder lacks the large amount of traditional hydrogen-bonding groups, like –OH and –COOH, the abundant imine groups in the repeating units and some terminal amine groups can also provide efficient interaction with Si surface. Molecular simulations and atomic force microscopy (AFM) measurements demonstrated that the intra- and intermolecular interactions between polymer chains and efficient interaction of polymers with Si surface both contribute to the improved binder performance.

2. Experimental section

2.1. Preparation of polyimine binder, electrodes

95Si/Polyimine electrode was prepared as follows: 5.7 mg of 4,4′-Biphenyldicarboxaldehyde (BCA, 0.027 mmol) (Tianjin Heowns Biochemical Technology Co., Ltd), 4.3 mg of 1,5-Naphthalenediamine (NDA, 0.027 mmol) (Tianjin Heowns Biochemical Technology Co., Ltd) and 0.2 mL of N-methyl pyrrolidone (NMP) (Tianjin Chemical Co. Lt) was added into the flask. The flask was degassed by three pump-thaw cycles and heated at 95 °C for 3 h with vigorous stirring under the argon atmosphere. After cooling down to the room temperature, 0.19 g of SiNPs (Aladdin, 30–60 nm, see Fig. S6 for SEM images) and another 1.5 mL NMP were added into the flask and after vigorous stirring for 2 h, the obtained slurry was cast on a copper foil and dried in a vacuum oven at 120 °C for 12 h. The electrodes with other Si ratio were prepared under the same condition by adjusting the weight ratio of SiNPs and monomers.

The electrodes based on PAA (Macklin, $M_w \approx 45{,}000$), CMC (CMC2200, DAICEL) and PVDF (Kynar HSV900, ARKEMA) were prepared by dispersing the SiNPs, binder and Super P carbon (SP) (TIMICAL SUPER C65) in NMP (deionized water for CMC) with a weight ratio of 70:15:15 or 95:2.5:2.5 and then processing slurry coating, drying and cutting process at the same condition. The electrode with PEDOT:PSS (MERYER, 1.5% in water) as the binder was prepared by dispersing the SiNPs and PEDOT:PSS in deionized water with a weight ratio of 95:5, and then using the same procedure as the electrodes with PAA, CMC and PVDF as the binder. The electrode with 100 wt% of Si was prepared by dispersing the SiNPs in NMP and then processing slurry coating, drying and cutting process at the same condition with other electrodes. The mass loading of all electrodes were around 0.5 mg/cm^2 based on the SiNPs.

2.2. Characterizations of binder and electrode materials

Scanning electron microscope (SEM, JSM-7800, JEOL, Japan), transmission electron microscopy (TEM, JSM-2800, JEOL, Japan) and energy dispersive X-ray spectrometer (EDX) were used to analyze the morphology, structure and element distributions. The X-ray diffraction (XRD) patterns were collected from the Rigaku D/MAX-2500 XRD diffractometer, two-theta was scanned from 5° to 90°. Fourier transform infrared (FTIR) spectra were recorded on a Nicolet iS50 FT-IR Specrometer (Thermo Scientific) with the scanning range was 4000–525 cm^{-1}. Thermogravimetric analysis (TGA) was observed with a Seiko Exstar 6000 instrument at a scanning rate of 10 °C/min under the N_2 atmosphere. The densities of the binders were determined from the mass (weight balance, Mettler Toledo New Classic MF Model MS105DU) to volume (gas pycnometer, Micromeretics Accupyc II 1340) ratio under the atmospheric pressure with the temperature of 20 °C. The glass transition temperature (T_g) of the polyimine was measured by temperature-modulated Differential Scanning Calorimetry (DSC, TA instrument Q1000) in the temperature range of −80 °C–250 °C. The atomic force microscopy (AFM) indentation was measured using Omega Scope, AIST-NT (Novato, US) scanning probe microscope. Force-distance curves were recorded using a calibrated CP-PNPS-SiO-E−5 triangular cantilever (resonance f = 67 kHz, spring constant k = 0.32 N/m, length L = 100 μm). The specially-prepared cantilevers feature a colloidal SiO_2 tip with the diameter of 15 μm in order to simulate the surface of SiNPs. Cantilever deflection is recorded as the probe approaches the polymer surface, makes contact (indentation depth of 20 nm), and is retracted (pulled off) back to the initial non-contacting state. The adhesion force (i.e., pull-off force) is determined by the product of the spring constant and maximum cantilever deflection during the retraction part of the force-distance curves. The reported adhesion forces correspond to the average of at least 30 repeated measurements conducted from different locations on the binder film surface for every sample.

2.3. Battery assemble and electrochemical measurements

The electrodes were cut into 1.32 cm^2 circular sheet to assemble the CR2032 coin cells (stainless steel CR-2032, Hohsen Corp., Osaka, Japan) with lithium metal (Tianjin Zhongneng Lithium Industry Co., Ltd, Diameter = 15 mm) as the counter electrode and polypropylene (Celgard 2400) as the separator. The electrolyte consisted of 1 M $LiPF_6$ in ethylene carbonate/diethyl carbonate (1 : 1 by volume) solution with 10 wt% fluoroethylene carbonate (FEC). The batteries assemble process was

conducted in Ar-fill glove box with H_2O and O_2 less than 1 ppm.

The galvanostatic test was obtained by using the LAND CT2001A battery test system under different current densities with the voltage range of 0.01–1.5 V. The C rate was set to be a little higher than the full lithiation capacity of Si as 4000 mAh g^{-1}. The long-term cycling performance was tested at the current density of 200 mA g^{-1} for initial 3 cycles and then at the high current densities, i.e. 1000 (C/4) or 2000 (C/2) mA g^{-1}. It should be noted that, the specific capacity in the cycling performance and rate capability means the delithiation capacity or charge capacity. The cyclic voltammetry (CV) and electrochemical impendence spectroscopy (EIS) were measured on the Zennium Pro Electrochemical System with the scanning speed of 0.1 mV/s and the frequency range of 10^{-1}-10^4 Hz at a 5 mV amplitude, respectively. The electrochemical impendence was measured with the cells at the fully delithiation state after different discharge/charge process. All the electrochemical results were obtained at 25 °C in a temperature-controlled chamber.

2.4. Molecular simulations

Simulations of the polymers were carried out using LAMMPS implementation of force fields derived from OPLS-96 [56]. The general equation for energy is shown as equation (1) below. This includes Lennard-Jones and coulombic interactions for non-bonded atoms, and harmonic bond lengths and angles for bond atoms. Dihedral terms are used to maintain the rigidity of the aromatic rings. For all functional groups in the polyimine molecule, the nearest analogue in the OPLS-96 database was used to derive the force fields. Charges on a small number of atoms were adjusted slightly such that each monomer unit and termination was charge neutral. A complete list of bond and charge parameters are shown in the supplemental material.

$$E = \sum_{i,j\ not\ bonded} \left\{ \varepsilon_{ij} \left[\left(\frac{\sigma_{ij}}{r_{ij}}\right)^{12} - 2\left(\frac{\sigma_{ij}}{r_{ij}}\right)^{6} \right] + \frac{1}{4\pi\varepsilon_0}\frac{q_i q_j}{r_{ij}} \right\} + \sum_{i,j\ bonded} k_{ij}\left(r_{ij} - r_{0,ij}\right)^2 + \sum_{i,\ j,\ k\ bonded} k_{ijk}\left(\theta_{ijk} - \theta_{0,ijk}\right)^2 + \sum_{i,j,k,l\ dihedral} \frac{V_{2,ijkl}}{2}\left[1 + \cos(2\varphi_i)\right] \quad (1)$$

The quartz surface was taken from Emami et al. [57], who uses Lennard-Jones, charges, and harmonic bonds and angle terms to simulate the quartz surface. The surface was made periodic in all directions, but the box length in the direction normal to the surface was set very large to avoid interactions between surface layers. A fully protonated surface was simulated. The surface was terminated at 4 layers of silica tetrahedra, and the charges on the bottom-most oxygens was adjusted such that the entire surface layer had neutral charge. This truncation did not significantly affect the silicon-oxide network structure. Mixing of Lennard-Jones parameters between the quartz surface and the polyimine polymer were carried out using the arithmetic approach ($\varepsilon_{ij} = \sqrt{\varepsilon_{ii}\varepsilon_{jj}}$ and $\sigma_{ij} = (\sigma_{ii} + \sigma_{jj})/2$). Geometric mixing was also tested and found to give similar results.

Simulations were run using Langevin dynamics with a 10 ns damping term. The structures were initially relaxed for 10 ns at 2000 K, then ramped down to 300 K and held for 10 ns. For polymer-polymer interactions, four polymers with a mixture of amine and methane terminations were simulated. For the quartz-surface a single polymer was simulated with an amine termination in proximity with the quartz surface.

3. Results and discussion

The synthesis of polyimine binder and the fabrication process of the electrode are schematically illustrated in Scheme 1a, where the 4, 4′-biphenyldicarboxaldehyde (BCA) and 1, 5-naphthalenediamine (NDA) were used without purification. After 3 h' condensation at 95 °C under argon (Ar) atmosphere, the obtained N-methyl pyrrolidone (NMP) solution of polyimine was directly mixed with Si nanoparticles (SiNPs), followed by the slurry-coating, drying and cutting process to afford the polyimine-containing Si electrodes. As shown in Fig. S1, the peak at 1645 cm^{-1} in the FTIR spectrum of polyimine indicates the formation of imine bond from the amine (780 cm^{-1}) and aromatic aldehyde (810 cm^{-1}) groups in the two precursors [58]. As illustrated by the molecular simulation in Scheme 1b, physical interactions including nitrogen-hydrogen bonds and aromatic carbon-hydrogen bonds are formed between the different polyimine chains, which results in a physically cross-linked three-dimensional (3D) conductive polymer network. The polyimine binder shows excellent thermal stability with the decomposition temperature of ~450 °C (Fig. S2a), and the DSC result reveals the glassy nature of polyimine with glass transition temperature (T_g) higher than 200 °C (Fig. S2b).

The electrochemical stability of polyimine was measured using the cyclic voltammetry (CV) at the scanning rate of 0.1 mV/s and 1 mV/s as shown in Fig. S3 and Fig. S4, respectively. The flat peak under the low scanning rate and good reproducibility of all the peaks under the high scanning rate suggested the stable electrochemical performance of polyimine in the tested voltage range. The cycling performance of the polyimine-only electrode was also measured at current density of C/20 (1 C = 4000 mA g^{-1}, the same below) in the potential window of 0.01–1.5 V as displayed in Fig. S5. Except for the initial discharge (lithiation) capacity of 111.6 mAh g^{-1}, the capacities of the following cycles are all less than 10 mAh g^{-1}, suggesting the negligible extent of lithium trapping to the polyimine binder. Scanning electron microscopy (SEM), scanning transmission electron microscopy (STEM) images (Fig. S6 a and b) of SiNPs reveal homogenous diameter distribution around 50 nm. The clear and sharp peaks in the XRD patterns displayed in Fig. S7 demonstrate the crystallinity nature of the SiNPs [59]. The energy dispersive X-ray spectrometer (EDX) mapping results (Figs. S6c–f) indicate the existence of the SiO_2 on the surface of the particles. According to previous reports, the abundant hydroxyl groups of the SiO_2 layer will contribute to form efficient interactions between the binder materials and SiNPs [60,61].

The electrochemical performance of the electrode with 70 wt% of the SiNPs and 30 wt% of the polyimine binder was initially evaluated. As shown in Fig. 1a, the 70Si/Polyimine electrode delivers an initial delithiation capacity of 3280.2 mAh g^{-1} at the current density of C/10 and a capacity retention of 85.6% after 100 cycles based on the 4th cycle (Table S1). In contrast, the Si electrodes using PAA (70Si/(PAA + SP)), CMC (70Si/(CMC + SP)) or PVDF (70Si/(PVDF + SP)) as binders (15 wt % for both binder content and SP content) show the capacity retention of only 45.2%, 52.1% and 8.0%, respectively, after 100 cycles. The long-term cycling performance of the electrodes with Si content of 70 wt% is displayed in Fig. 1e. The 70Si/Polyimine electrode exhibited a delithiation capacity of 800.1 mAh g^{-1} and capacity retention of 82.4% after 1000 cycling at the current density of 1 C. In contrast, the electrodes with PAA and PVDF as binders show rapid capacity fading. The reversible specific capacity was observed decreasing from ~3300 mAh g^{-1} to ~930 mAh g^{-1} and then bumping up to ~3100 mAh g^{-1} when the current densities were increased from C/20 to 2.5 C and switched back to C/20 (Fig. 1b), which suggested an excellent rate performance of the polyimine-containing Si electrode. Electrode with CMC binder shows comparable or even slightly higher capacity than the electrode with polyimine binder at high charging/discharging rates. Higher viscosity of CMC solution and the abundant –OH groups in the CMC molecules may result a homogenous slurry, porous electrode coating and enhanced adhesion with the current collector, which should contribute to the CMC-binder containing Si electrode with relative improved electrochemical performance at high charging rate [39]. The superior cycling performance and excellent rate capability of the 70Si/Polyimine electrode may be due to the fast lithium ion and electron transport in the conductive network formed by the polyimine binder. However, with only 70 wt% of active material in the 70Si/Polyimine electrode, the energy density normalized to the total electrode mass (total $= m_{binder} + m_{Si}$) is still limited, i.e., ~1400 mAh g^{-1}_{total} after 200 cycles with specific

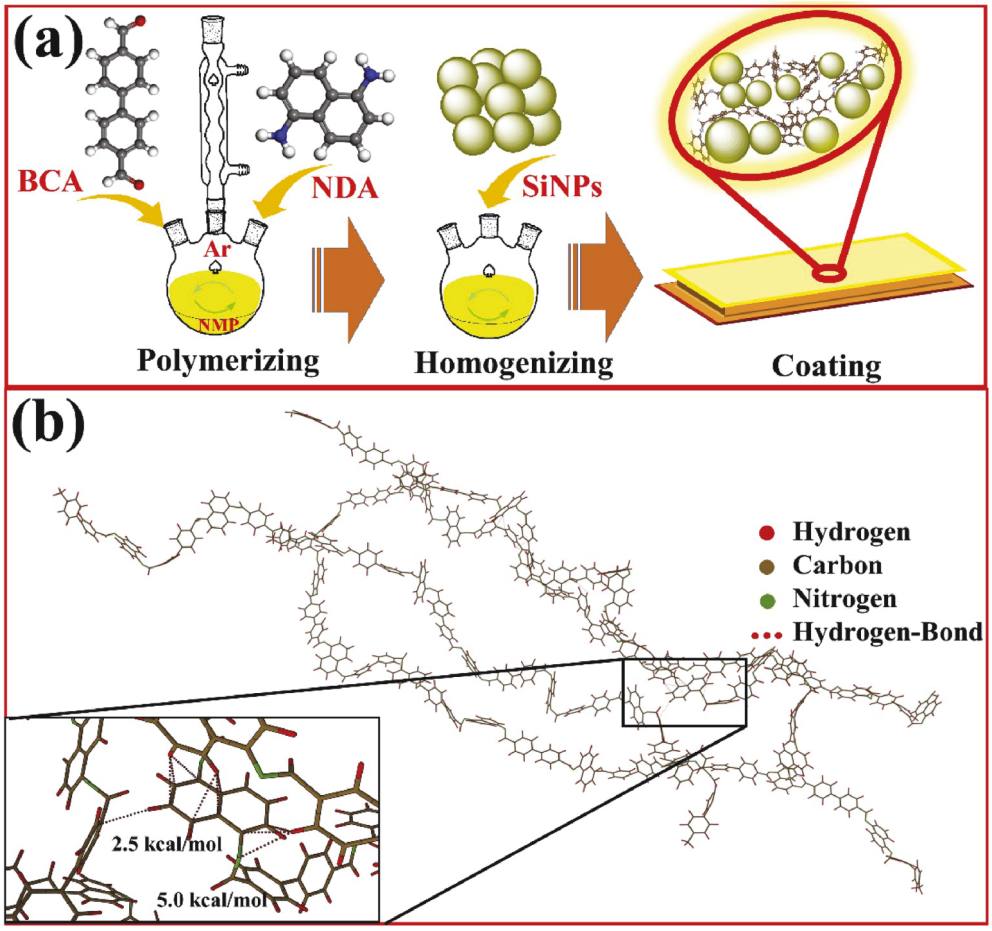

Scheme 1. (a) Schematic illustration of the electrode fabrication process. (b) Molecular simulation of polyimine.

capacity reaching 2005.3 mAh g^{-1}.

To further demonstrate the efficiency of polyimine binder, the electrodes with different Si contents (xSi/Polyimine, x = 90, 95, 96, 97 and 100), i.e., improved $R_{A/I}$ values, were also prepared and the electrochemical performance are displayed in Fig. 1c and d. It worth noticing that the total-electrode-mass normalized energy densities should also improve with increased Si content. As observed in Fig. 1c, the delithiation capacities of Si electrodes decreased gradually with increased Si contents, illustrating the increased ratio of "dead" Si during the delithiation/lithiation process due to the reduced density of continuous current paths [47]. The significantly improved cycling performance obtained for the xSi/Polyimine electrodes (x = 70, 90, 95, 96, and 97) compared with the electrode without any binder (100Si/Polyimine) demonstrated the vital role of polyimine as both binder material and conductive additive in the Si electrodes. For better comparison, the specific capacity is normalized to the total mass of electrode (SiNPs + Polyimine) as shown in Fig. 1d. In this aspect, the electrode 95Si/Polyimine ($R_{A/I}$ = 19) delivers the highest specific capacity and capacity retention of 2007.0 mAh g_{total}^{-1} and 80.4% (based on the 4th cycle), respectively, after 200 cycles (Fig. S8a). The initial Coulombic efficiencies of xSi/Polyimine electrodes with x = 70, 90, 95, 96, and 97 are 53.11%, 75.65%, 65.15%, 73.97% and 66.53%, respectively. One of the major reasons for their low initial Coulombic efficiency should be the electrochemically active nature of the polyimine, which exhibited an initial discharge capacity of 111.6 mAh g^{-1} as shown in Fig. S5. Moreover, the consumption of large amount of Li for the formation of a SEI layer and conductive network may also affect its initial Coulombic efficiency. In the subsequent cycles (after 10 cycles), the Coulombic efficiencies of all xSi/Polyimine electrodes are higher than 97% with high reversibility during the cycling process, indicating the formation of a relatively stable SEI layer (Fig. S8b). The high specific capacity, enhanced cycling stability and especially with the ultrahigh Si content make the 95Si/Polyimine electrode being superior among these Si electrodes. Therefore, the electrode with the Si ratio of 95 wt% ($R_{A/I}$ = 19) was chosen for further studies.

The surface morphology of fabricated 95Si/Polyimine electrodes was characterized by SEM, STEM and EDX as shown in Fig. 2a–c. The existence of the binder should contribute to the formation of uniform Si-electrode coating on the current collector, and the obtained porous structure may accommodate the volume variation during the charging-discharging process. The EDX mapping of the pristine electrode in Fig. 2d also reveals the uniform distribution of carbon and silicon, indicating the homogeneous distribution of conductive polymers and active materials. With 5.6 wt% of carbon from conductive polymers and 81.5 wt% of silicon and 12.6 wt% of oxygen mostly from SiNPs, the map sum spectrum confirms the high weight ratio of the active materials (Fig. 2dIV). The oxidation of Si surface and depth of element measurement (several nanometers to a few of micrometers) should be the reason of relatively lower weight ratio of silicon element than the actual value. Besides, the lower density of polyimine (1.31 g cm^{-3}) compared with other binders like PAA (1.51 g cm^{-3}), CMC (1.65 g cm^{-3}) and PVDF (1.85 g cm^{-3}) (Table S2) may also contributes to the complete coverage of polyimine binder on the SiNPs, thus improving the electrochemical performance of the resulting electrode with such a low weight ratio of polyimine binder.

The CV curves for the first three cycles of the 95Si/Polyimine electrode in the voltage range of 0.01–1.5 V were shown in Fig. S9. In the initial cathodic scan, due to the crystallinity of Si, only one peak was observed at ~0.06 V [8]. After the initial lithiation process, the crystalline Si was transferred to amorphous silicide. The cathodic peak

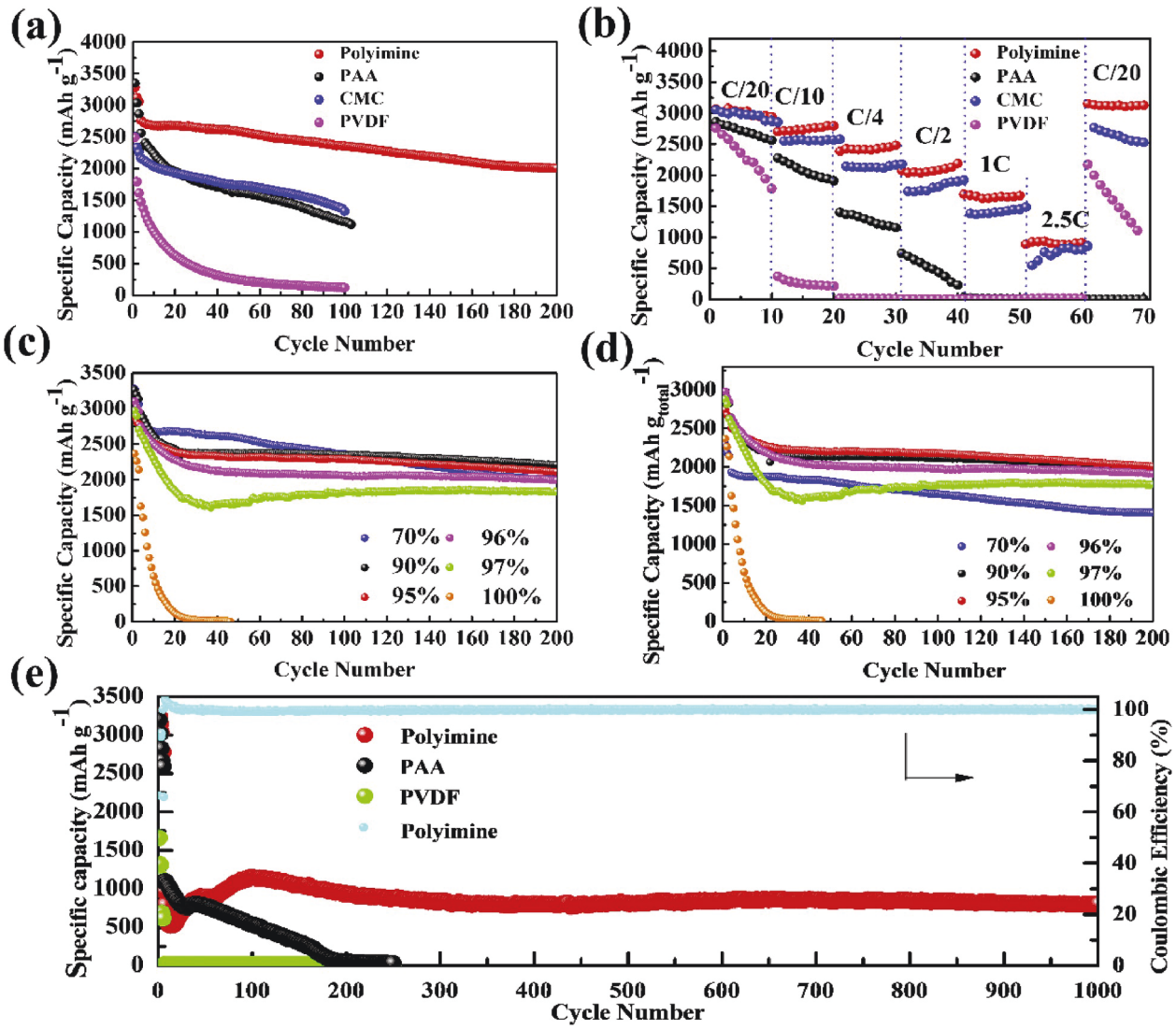

Fig. 1. Electrochemical performance of the electrodes with different binders: (a) Cycling performance of the 70Si/(Binder + SP) (Binder = PAA, CMC and PVDF. With polyimine as binder, there is 30 wt% of polyimine in the electrode without any SP) electrodes. (b) Rate capability of the 70Si/(Binder + SP) electrodes under different C rates. (c) Cycling performance of the xSi/Polyimine (x = 70, 90, 95, 96, 97 and 100) electrodes at the current density of C/10. (d) Specific capacity of the xSi/Polyimine (x = 70, 90, 95, 96, 97 and 100) electrodes normalized to the total electrode mass (Si + Polyimine) at the current density of C/10. (e) Long-term cycling performance of the 70Si/Polyimine electrode at the current density of 1 C.

located at ~0.21 V and anodic peaks located at ~0.32 and ~0.49 V are characteristic of amorphous Si in the subsequent cycles [26]. The electrochemical performance of the Si based electrodes with different binders but the same silicon content, i.e., the same $R_{A/I}$ value, were evaluated by half cells with Li metal as the counter electrode. As displayed in Fig. 3a, the specific delithiation capacity of the 95Si/Polyimine electrode ($R_{A/I}$ = 19) delivered the highest specific capacity of 2112.6 mAh g^{-1} and the capacity retention of 80.4% (based on the 4th cycle) at the current density of C/10 after 200 cycles. By contrast, the electrodes with other binders or without any binders (Super P carbon, SP only) show rapid capacity fading. Especially, the PEDOT:PSS, which has been widely reported to show superior binder performance for Si electrodes [50,62,63], was also evaluated for the electrode with high $R_{A/I}$ values. As shown in Fig. 3a, when the $R_{A/I}$ value reaching 19, the Si electrode with PEDOT:PSS binder exhibited huge irreversible specific capacity loss with the delithiation capacity of only 624.3 mAh g^{-1} after 200 cycles. The rapid capacity fading of Si electrodes with high $R_{A/I}$ value using these polymer materials, including PAA, CMC, PVDF and PEDOT:PSS, may be due to the low electronic/ionic conductivity and weak interactions between the SiNPs, conductive network and the current collector. Moreover, the electrochemical performance of electrodes with high silicon contents in previous reports has also been summarized in Table S3. Among electrodes with various binders, the electrodes with polyimine binder show the highest Si content of 95 wt% ($R_{A/I}$ = 19) and one of the highest specific capacities normalized to the mass of the total electrode mass [47,51–53,61,62]. Although the Si electrode using poly(1-pyrenemethyl methacrylate-co-methacrylic acid) as the binder was reported to show slightly higher specific capacity [52], its capacity retention was much lower than the current system (74.59% @100 cycles based on the 5th cycle with 90 wt% Si, $R_{A/I}$ = 9 *vs* 80.42% @200 cycles based on the 4th cycle with 95 wt% Si, $R_{A/I}$ = 19). The comparative electrochemical performance demonstrates the superior binder performance of polyimine for high Si-content electrode.

The rate capability of the high-$R_{A/I}$ electrodes with different binders are displayed in Fig. 3b, and a reversible specific capacity of ~2330, 2146, 2002, 1915, 1828, 1590 and 1415 mAh g^{-1} can be obtained at the current densities of C/20, C/10, C/7, C/5, C/4, C/2.5 and C/2, respectively, for the 95Si/Polyimine electrode. More importantly, after multiple high current density discharging-charging cycles, a reversible specific capacity of ~2130 mAh g^{-1} can still be recovered when the

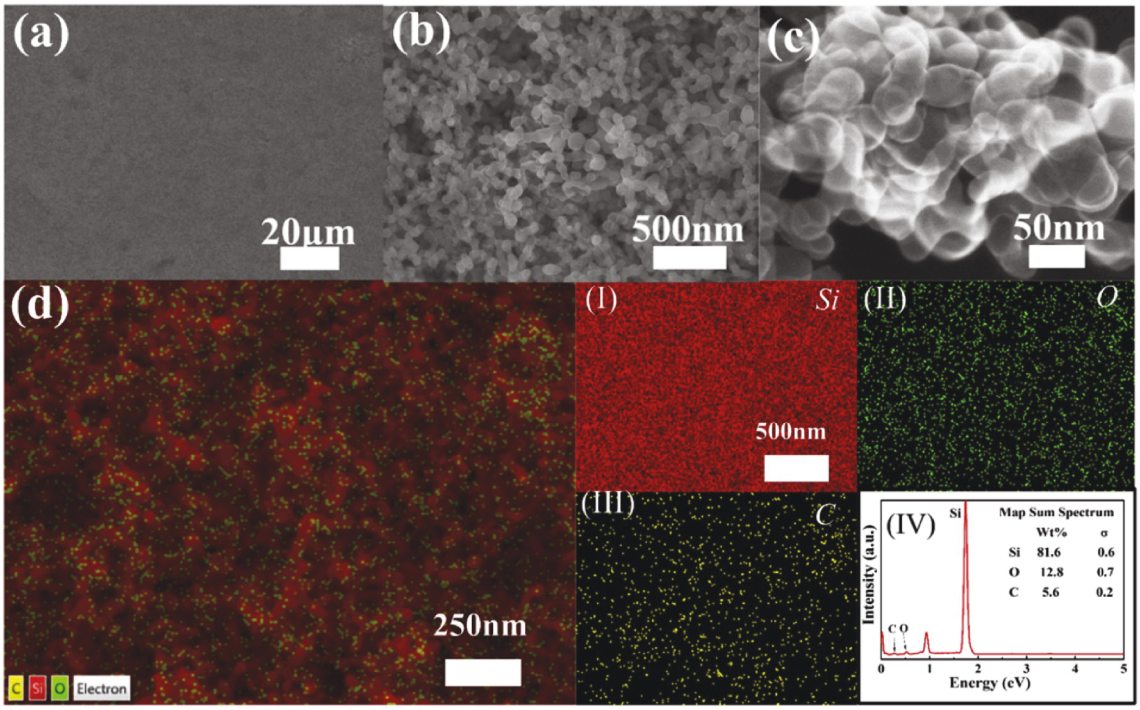

Fig. 2. Surface morphology of the 95Si/Polyimine electrodes. SEM images of pristine electrodes with low (a) and high (b) resolution, (c) STEM images of pristine electrodes, (d) EDX mapping images of Si (I), oxygen (II) and carbon (IV), (IV) is the corresponding EDX spectrum.

current density decreased to the initial C/20. Even at the high current density of 1.25 C, a specific capacity of ~433 mAh g^{-1} can still be retained. At the same condition, the high-$R_{A/I}$ electrodes with other binders exhibit rapid capacity fading despite high initial delithiation capacities. The EIS results show that the impedance did not increase significantly within 100 cycles, indicating the formation of a stable SEI layer. After a long-time discharge/charge process, i.e., more than 100 cycles, the SEI layer started to deteriorate, rendering the increased electrochemical impendence. Therefore, higher electrochemical impedance was obtained after 200 cycles comparing with that after 100 cycles as shown in Fig. 3c [64]. The long-term cycling performance of the 95Si/Polyimine electrodes at the current density of C/4 and C/2 was shown in Fig. 3d. It can be seen that even after 500 cycles, the reversible specific capacities of 1442 and 1087.8 mAh g^{-1} can be retained at the current densities of C/4 and C/2, respectively. The specific capacity decreased in initial cycles and then increased after a few cycles should be due to the electrode polarization at the high current densities [65]. These results suggested excellent Li^+ and electron transfer capability and highly stable structure of the Si electrode arising from the polyimine binder.

To better understand the physical/chemical effect of polyimine binder on the Si electrode, the overall morphology of the electrodes after 100 discharge-charge cycles with different binders were characterized by SEM and displayed in Fig. 4. For the 95Si/Polyimine electrode as shown in Fig. 4a, after 100 delithiation/lithiation repeated cycles, a crack-free surface was clearly observed. On the other hand, for the high Si-content electrodes ($R_{A/I}$ = 19) with PAA, CMC and PVDF as binders, large cracks can be observed after 100 cycles at the same current density (C/4, Fig. 4b, c and d). The mechanical instability of electrodes may render the isolation of Si from the conductive network, thus leading to poor electrochemical performance [66–69]. The electrochemical impendence spectroscopy (EIS) performed after different cycles (current density of C/10, Fig. 3c) of 95Si/Polyimine electrode reveals no significant increase of the resistance, which indicates the formation of a stable SEI layer during the cycling process [70]. In this regard, the polyimine binder plays a vital role in retaining a stable conductive network and SEI layer for high Si-content electrodes. Its superior performance can be attributed to its unique properties, including the low density, capability of forming porous architecture and enhanced interaction with Si surface.

Molecular simulations (LAMMPS) were conducted to calculate the interactions among the different polyimine chains and between polyimine and the SiNPs. According to Jeffrey's categorization [71], hydrogen bonds can be categorized into long, medium, and short bond-lengths, where a shorter length corresponds to a stronger bonding force. As shown in Scheme 1b, Fig. S10 and Fig. 5, numerous medium-length hydrogen bonds formed in the polymer-polymer and polymer-silicate surface simulations. In the polymer-polymer simulations, the binding energy of nitrogen-hydrogen bonds is 5.0 kcal/mol, and the hydrogen bonds between the aromatic rings and nearby hydrogen group is 2.5 kcal/mol. Although the nitrogen-hydrogen bonds (Fig. 5a–I) are more stable than the aromatic carbon-hydrogen bonds (Fig. 5a–II), the presence of large number of aromatic rings leads to the aromatic carbon-hydrogen bonds dominating the physical interactions between the polymer and Si surface (see comparative ratios in Table S4). Moreover, hydrogen bonds between the oxygen of Si surface and the polymer hydrogens also form but they are less stable than the above two bonds due to the relatively longer distance between the two atoms. The polymer chains are oriented by the N–H hydrogen bonds and aromatic carbon-hydrogen bonds, causing the intermediate carbons to orient upward (see Fig. 5IV). There are more hydrogen bonds form between the polymer and the Si-surface, which is consistent to previous results shown for polyethyleneimine that can strongly binds silicate surfaces [72]. To further study the functionalities of synthesized polyimine as polymer binder in Si electrodes, the adhesion force between Si surface and polymeric materials was experimentally evaluated using the AFM. The EDX mapping results in Fig. 2 demonstrated the abundant oxygen element on the Si nanoparticles, manifesting the presence of SiO_2 at the surface. To evaluate the adhesion force between the Si particles and polymer binder, an AFM cantilever equipped with a SiO_2 colloidal tip (diameter of 15 μm) as the probe was used (Fig. 5b). By retracting from the polymer surface, the adhesion forces between the polymer surface and SiO_2 colloidal tip can be collected. In this test, higher adhesion force indicated more interactions between the polymer binder and Si particles, which should contribute to effectively accommodate the volume

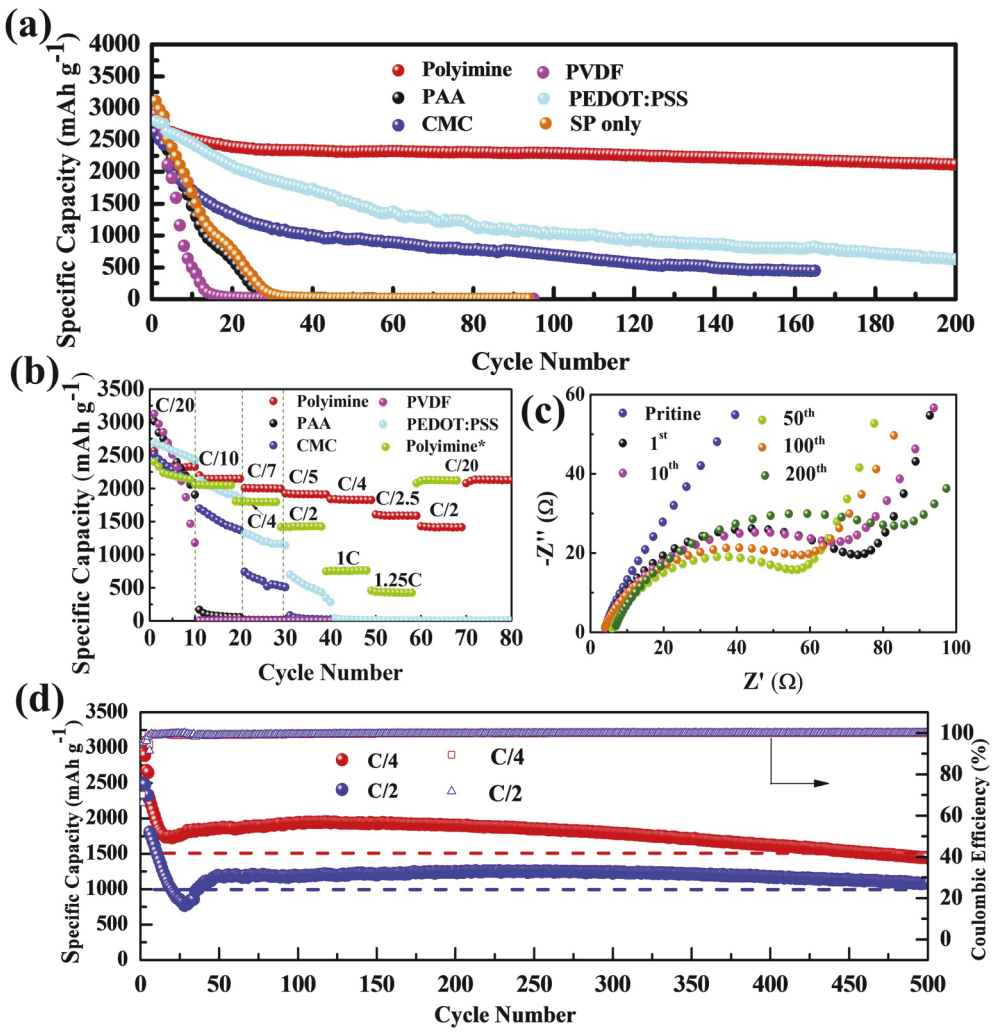

Fig. 3. Electrochemical performance of the electrodes with different binders ($R_{A/I} = 19$). (a) Cycling performance and (b) rate capability of the electrodes with different binders. The electrodes with Polyimine, PAA, CMC, PVDF and PEDOT:PSS as binder have the same current density. The Polyimine*-based electrode has different charging rate. (c) EIS profiles of the 95Si/Polyimine electrode after charging to 1.5 V with different cycles. (d) The long-term cycling performance of the 95Si/Polyimine electrode.

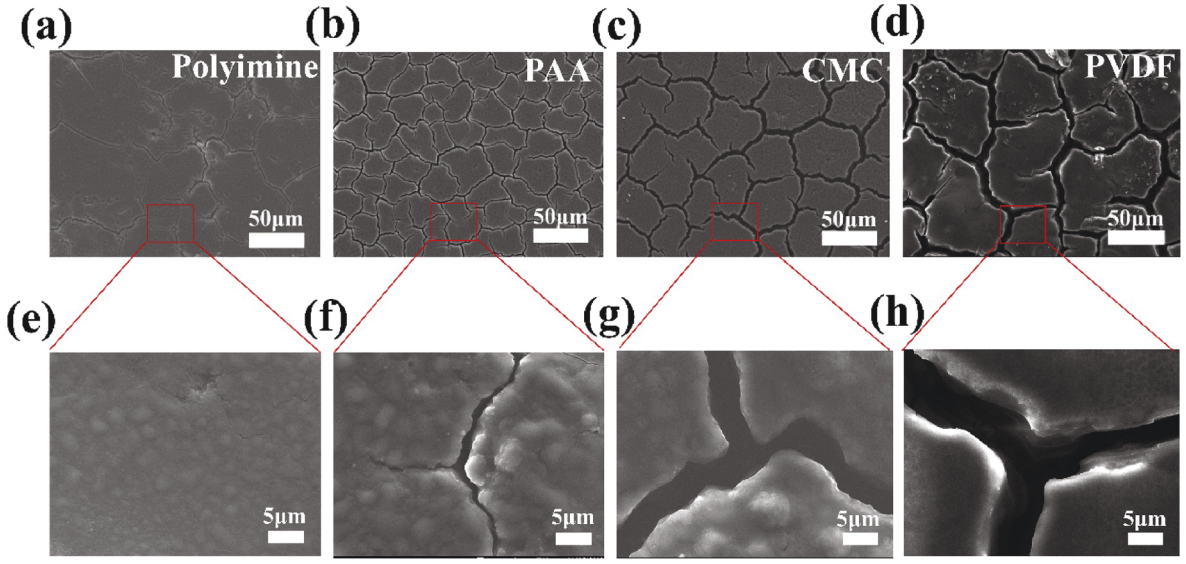

Fig. 4. SEM images of the electrodes with different binders after 100 cycles. (a) Polyimine, (b) PAA, (c) CMC (d) PVDF. (e, f, g and h) are the zoom-in area of a, b, c and d, respectively.

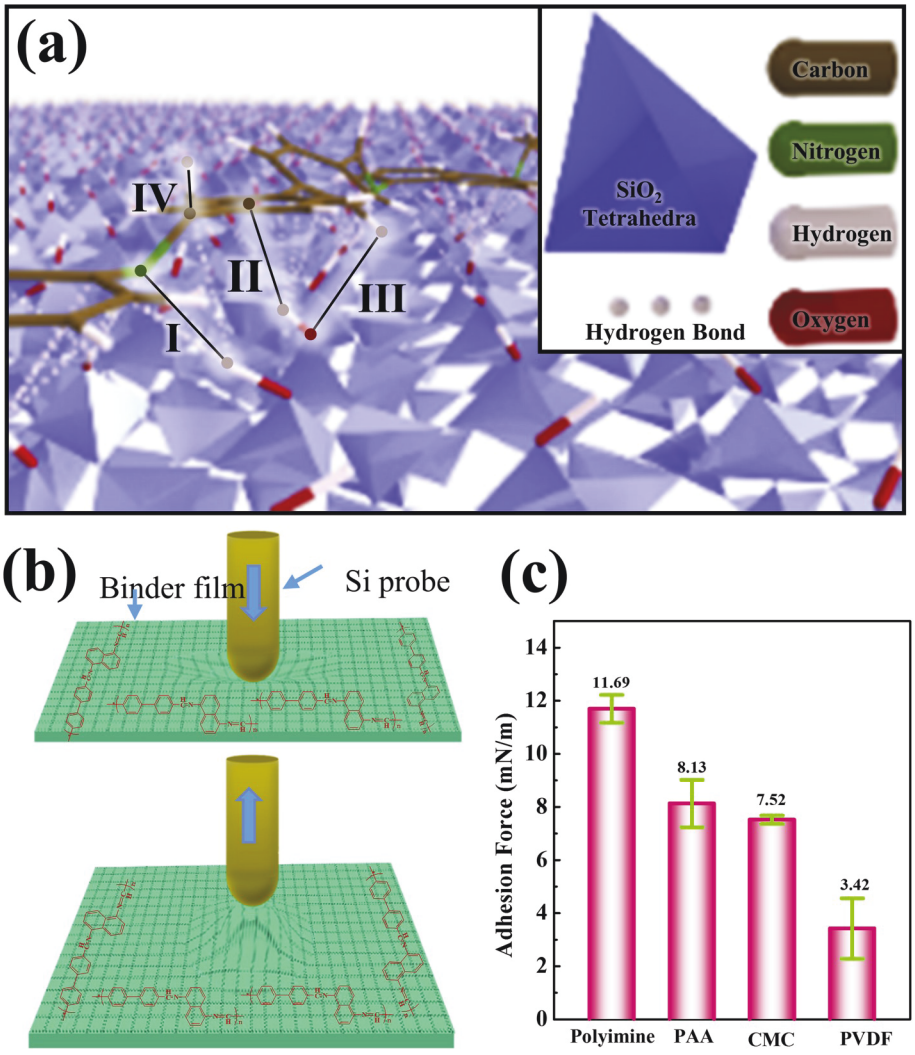

Fig. 5. (a) Molecular simulation shows that extensive hydrogen-bonding between the polymer and the –OH terminated quartz surface: (I) nitrogen-hydrogen bonds between the polymer chains and Si surface. (II) coulombic interaction between the aromatic rings and the terminal hydrogens on Si surface; (III) hydrogen bonds between the terminal hydrogen and the surface oxygen; (IV) upwards orientation of the neighboring carbon-hydrogens due to the strong nitrogen-hydrogen bonds. (b) The schematic diagram of the AFM test. (c) Comparison of the average Si-polymer adhesion forces for different polymer binders determined from the pull-off force of an AFM colloidal probe. Note that the forces are normalized by the probe diameter.

variation during the repeated delithiation/lithiation process, leading to enhanced electrochemical performance. As shown in Fig. 5c, due to weak van der Waals interactions between the SiO_2 probe and PVDF film, the average adhesion force is only 3.4 mN/m. While for PAA and CMC, comparable higher adhesion forces can be observed (8.1 and 7.5 mN/m, respectively), due to the presence of polar group in both polymers. In the respect of polyimine, due to the enhanced physical interactions between polyimine and SiO_2 probe (even without well-demonstrated functional groups like PAA and CMC), further improved adhesion force of 11.7 mN/m was achieved [67,73]. The results are consistent with the cycling performance in Fig. 3 and the SEM images in Fig. 4. Due to the combination of a dynamic network formed by physically cross-linked linear polymers with extensive hydrogen bonds between the polyimine molecules and Si surface [32], the high Si-content electrodes assembled with polyimine binder can endure dramatic volume changes and maintain the electronic conduction of Si during the repeated lithiation/delithiation process, thereby ensuring a stable cycling performance.

4. Conclusion

In summary, a polyimine binder with facile synthesis method and ultra-efficient binder performance was demonstrated, which firstly enable a slurry-coating electrode with unprecedentedly high $R_{A/I}$ value (up to 19) and long cycle life (500–1000 cycles). The polyimine binder enables the 70Si/Polyimine electrode with retention capability of 2005.3 mAh g^{-1} after 200 cycles at C/10 and capacity retention of 82.4% after 1000 cycles at C/2. More importantly, the electrode 95Si/Polyimine ($R_{A/I} = 19$) also delivers a delithiation capacity of 2114 mAh g^{-1} and capacity retention of 80.4% after 200 cycles at the current density of C/10 (400 mA g^{-1}). After 500 continuously deep cycles at the current density of C/2, a delithiation capacity of 1087.8 mAh g^{-1} can still be obtained. Physical cross-linking of the conductive network and efficient interactions with the Si surface revealed by molecular simulations and AFM analysis indicate the formation of stable solid electrolyte interphase layer and a mechanically robust network.

The ultra-efficient binder performance was demonstrated by enabling the Si electrode with high $R_{A/I}$ value and stable cycling performance, which suggest the electrochemical performance of Si (or Si composite) electrodes can be significantly improved using a small amount of polyimine binder. Considering the simple synthesis method and ultra-efficient binder performance, the developed polyimine binder will be useful in achieving the Si (or Si composite) electrodes with high cost efficiency and long cycle life, and become the game-changer “inert” material for next-generation energy-storage devices. The concept demonstrated here may also aid the design of other types of high-performance energy-storage devices.

Declaration of competing interest

The authors declare that they have no known competing financial

interests or personal relationships that could have appeared to influence the work reported in this paper.

CRediT authorship contribution statement

Shilun Gao: Data curation, Writing - original draft, Writing - review & editing. **Feiyuan Sun:** Writing - review & editing, Data curation. **Alexander Brady:** Software, Writing - review & editing. **Yiyang Pan:** Writing - review & editing. **Andrew Erwin:** Supervision, Validation. **Dandan Yang:** Writing - review & editing. **Vladimir Tsukruk:** Supervision, Validation. **Andrew G. Stack:** Software, Supervision. **Tomonori Saito:** Software, Supervision. **Huabin Yang:** Conceptualization, Funding acquisition, Writing - review & editing. **Peng-Fei Cao:** Conceptualization, Funding acquisition, Writing - original draft.

Acknowledgements

This work was financially supported by the Natural Science Foundation of China (21421001), the Natural Science Foundation of Tianjin, China (18JCZDJC31400), the MOE Innovation Team (IRT13022) and the Ph.D. Candidate Research Innovation Fund of NKU School of Materials Science and Engineering. P.-F. Cao and T. Saito also acknowledges partial financial support on binder development by the US Department of Energy, Office of Science, Basic Energy Science, Material Science, and Engineering Division. A. Brady and A. Stack were supported by the U.S. Department of Energy, Office of Science, Office of Basic Energy Sciences, Chemical Sciences, Geosciences, and Biosciences Division.

Appendix A. Supplementary data

Supplementary data to this article can be found online at https://doi.org/10.1016/j.nanoen.2020.104804.

References

[1] T.H. Wu, Y. Zhang, Z.D. Althouse, N. Liu, Nanoscale design of zinc anodes for high-energy aqueous rechargeable batteries, Mater. Today Nano 6 (2019), 100032.
[2] Y. Huang, H. Yang, Y. Zhang, Y. Zhang, Y. Wu, M. Tian, P. Chen, R. Trout, Y. Ma, T.-H. Wu, Y. Wu, N. Liu, A safe and fast-charging lithium-ion battery anode using MXene supported Li_3VO_4, J. Mater. Chem. A 7 (2019) 11250–11256.
[3] Y.-C. Zhang, Y. You, S. Xin, Y.-X. Yin, J. Zhang, P. Wang, X.-s. Zheng, F.-F. Cao, Y.-G. Guo, Rice husk-derived hierarchical silicon/nitrogen-doped carbon/carbon nanotube spheres as low-cost and high-capacity anodes for lithium-ion batteries, Nano Energy 25 (2016) 120–127.
[4] X. Zuo, J. Zhu, P. Müller-Buschbaum, Y.-J. Cheng, Silicon based lithium-ion battery anodes: a chronicle perspective review, Nano Energy 31 (2017) 113–143.
[5] T. Liu, C.-J. Tong, B. Wang, L.-M. Liu, S. Zhang, Z. Lin, D. Wang, J. Lu, Trifunctional electrode additive for high active material content and volumetric lithium-ion electrode densities, Adv. Energy Mater. 9 (2019) 1803390.
[6] F.A. Soto, P. Yan, M.H. Engelhard, A. Marzouk, C. Wang, G. Xu, Z. Chen, K. Amine, J. Liu, V.L. Sprenkle, F. El-Mellouhi, P.B. Balbuena, X. Li, Tuning the solid electrolyte interphase for selective Li- and Na-ion storage in hard carbon, Adv. Mater. 29 (2017) 29–1606860.
[7] H. Jia, J. Zheng, J. Song, L. Luo, R. Yi, L. Estevez, W. Zhao, R. Patel, X. Li, J.-G. Zhang, A novel approach to synthesize micrometer-sized porous silicon as a high performance anode for lithium-ion batteries, Nano Energy 50 (2018) 589–597.
[8] A. Magasinski, P. Dixon, B. Hertzberg, A. Kvit, J. Ayala, G. Yushin, High-performance lithium-ion anodes using a hierarchical bottom-up approach, Nat. Mater. 9 (2010) 353–358.
[9] I. Kovalenko, B. Zdyrko, A. Magasinski, B. Hertzberg, Z. Milicev, R. Burtovyy, I. Luzinov, G. Yushin, A major constituent of Brown algae for use in high-capacity Li-ion batteries, Science 334 (2011) 75–79.
[10] J. Lopez, D.G. Mackanic, Y. Cui, Z. Bao, Designing polymers for advanced battery chemistries, Nat. Rev. Mater. 4 (2019) 312–330.
[11] X. Li, P. Meduri, X. Chen, W. Qi, M.H. Engelhard, W. Xu, F. Ding, J. Xiao, W. Wang, C. Wang, J.-G. Zhang, J. Liu, Hollow core–shell structured porous Si–C nanocomposites for Li-ion battery anodes, J. Mater. Chem. 22 (2012) 11014–11017.
[12] Y. Sun, N. Liu, Y. Cui, Promises and challenges of nanomaterials for lithium-based rechargeable batteries, Nat. Energy 1 (2016) 16071.
[13] Y. Sun, J. Lopez, H.W. Lee, N. Liu, G. Zheng, C.L. Wu, J. Sun, W. Liu, J.W. Chung, Z. Bao, Y. Cui, A stretchable graphitic carbon/Si anode enabled by conformal coating of a self-healing elastic polymer, Adv. Mater. 28 (2016) 2455–2461.
[14] B. Zhu, N. Liu, M. McDowell, Y. Jin, Y. Cui, J. Zhu, Interfacial stabilizing effect of ZnO on Si anodes for lithium ion battery, Nano Energy 13 (2015) 620–625.
[15] H. Wu, G. Yu, L. Pan, N. Liu, M.T. McDowell, Z. Bao, Y. Cui, Stable Li-ion battery anodes by in-situ polymerization of conducting hydrogel to conformally coat silicon nanoparticles, Nat. Commun. 4 (2013) 1943.
[16] Z. Xu, J. Yang, T. Zhang, Y. Nuli, J. Wang, S.-i. Hirano, Silicon microparticle anodes with self-healing multiple network binder, Joule 2 (2018) 950–961.
[17] T. Liu, Q. Chu, C. Yan, S. Zhang, Z. Lin, J. Lu, Interweaving 3D network binder for high-areal-capacity Si anode through combined hard and soft polymers, Adv. Energy Mater. 9 (2019), 1802645.
[18] X. Chen, X. Li, D. Mei, J. Feng, M.Y. Hu, J. Hu, M. Engelhard, J. Zheng, W. Xu, J. Xiao, J. Liu, J.G. Zhang, Reduction mechanism of fluoroethylene carbonate for stable solid-electrolyte interphase film on silicon anode, Chem. Sus. Chem. 7 (2014) 549–554.
[19] L. Zong, B. Zhu, Z. Lu, Y. Tan, Y. Jin, N. Liu, Y. Hu, S. Gu, J. Zhu, Y. Cui, Nanopurification of silicon from 84% to 99.999% purity with a simple and scalable process, Proc. Natl. Acad. Sci. U. S. A. 112 (2015) 13473–13477.
[20] T. Zhang, Z. Xu, Y. Guo, C. Liang, J. Wang, J. Yang, Building high performance silicon–oxygen and silicon–sulfur battery by in-situ lithiation of fibrous Si/C anode, J. Alloys Compd. 806 (2019) 335–342.
[21] L. Wei, Z. Hou, High performance polymer binders inspired by chemical finishing of textiles for silicon anodes in lithium ion batteries, J. Mater. Chem. A 5 (2017) 22156–22162.
[22] F.-H. Du, K.-X. Wang, J.-S. Chen, Strategies to succeed in improving the lithium-ion storage properties of silicon nanomaterials, J. Mater. Chem. A 4 (2016) 32–50.
[23] X. Su, Q. Wu, J. Li, X. Xiao, A. Lott, W. Lu, B.W. Sheldon, J. Wu, Silicon-based nanomaterials for lithium-ion batteries: a review, Adv. Energy Mater. 4 (2014), 1300882.
[24] F. Dai, J. Zai, R. Yi, M.L. Gordin, H. Sohn, S. Chen, D. Wang, Bottom-up synthesis of high surface area mesoporous crystalline silicon and evaluation of its hydrogen evolution performance, Nat. Commun. 5 (2014) 3605.
[25] D. Tang, R. Yi, M.L. Gordin, M. Melnyk, F. Dai, S. Chen, J. Song, D. Wang, Titanium nitride coating to enhance the performance of silicon nanoparticles as a lithium-ion battery anode, J. Mater. Chem. A 2 (2014) 10375–10378.
[26] X. Li, M. Gu, S. Hu, R. Kennard, P. Yan, X. Chen, C. Wang, M.J. Sailor, J.G. Zhang, J. Liu, Mesoporous silicon sponge as an anti-pulverization structure for high-performance lithium-ion battery anodes, Nat. Commun. 5 (2014) 4105.
[27] S. Jeong, X. Li, J. Zheng, P. Yan, R. Cao, H.J. Jung, C. Wang, J. Liu, J.-G. Zhang, Hard carbon coated nano-Si/graphite composite as a high performance anode for Li-ion batteries, J. Power Sources 329 (2016) 323–329.
[28] L. Luo, H. Yang, P. Yan, J.J. Travis, Y. Lee, N. Liu, D.M. Piper, S.H. Lee, S. M. George, J.G. Zhang, Y. Cui, S. Zhang, C. Ban, C.M. Wang, Surface-coating regulated lithiation kinetics and degradation in silicon nanowires for lithium ion battery, ACS Nano 9 (2015) 5559–5566.
[29] Y. Zhang, N. Liu, Nanostructured electrode materials for high-energy rechargeable Li, Na and Zn batteries, Chem. Mater. 29 (2017) 9589–9604.
[30] T.W. Kwon, J.W. Choi, A. Coskun, The emerging era of supramolecular polymeric binders in silicon anodes, Chem. Soc. Rev. 47 (2018) 2145–2164.
[31] M. Ko, S. Chae, J. Ma, N. Kim, H.-W. Lee, Y. Cui, J. Cho, Scalable synthesis of silicon-nanolayer-embedded graphite for high-energy lithium-ion batteries, Nat. Energy 1 (2016) 16113.
[32] Y. Pan, S. Gao, F. Sun, H. Yang, P. Cao, Polymer binders constructed via dynamic non-covalent bonds for high-capacity silicon-based anodes, Chem. Eur J. 25 (2019) 10976–10994.
[33] M. Wu, X. Song, X. Liu, V. Battaglia, W. Yang, G. Liu, Manipulating the polarity of conductive polymer binders for Si-based anodes in lithium-ion batteries, J. Mater. Chem. A 3 (2015) 3651–3658.
[34] K. Grygiel, J.-S. Lee, K. Sakaushi, M. Antonietti, J. Yuan, Thiazolium poly(ionic liquid)s: synthesis and application as binder for lithium-ion batteries, ACS Macro Lett. 4 (2015) 1312–1316.
[35] H. Chen, M. Ling, L. Hencz, H.Y. Ling, G. Li, Z. Lin, G. Liu, S. Zhang, Exploring chemical, mechanical, and electrical functionalities of binders for advanced energy-storage devices, Chem. Rev. 118 (2018) 8936–8982.
[36] P. Sengodu, A.D. Deshmukh, Conducting polymers and their inorganic composites for advanced Li-ion batteries: a review, RSC Adv. 5 (2015) 42109–42130.
[37] M. Ling, J. Qiu, S. Li, C. Yan, M.J. Kiefel, G. Liu, S. Zhang, Multifunctional SA-PProDOT binder for lithium ion batteries, Nano Lett. 15 (2015) 4440–4447.
[38] P.F. Cao, M. Naguib, Z. Du, E. Stacy, B. Li, T. Hong, K. Xing, D.N. Voylov, J. Li, D. L. Wood, A.P. Sokolov, J. Nanda, T. Saito, Effect of binder architecture on the performance of silicon/graphite composite anodes for lithium ion batteries, ACS Appl. Mater. Interfaces 10 (2018) 3470–3478.
[39] R.B.L. Jing Li, J.R. Dahn, Sodium carboxymethyl cellulose A potential binder for Si negative electrodes for Li-ion batteries, Electrochem. Solid State Lett. 10 (2007) A17–A20.
[40] A. Magasinski, B. Zdyrko, I. Kovalenko, B. Hertzberg, R. Burtovyy, C.F. Huebner, T. F. Fuller, I. Luzinov, G. Yushin, Toward efficient binders for Li-ion battery Si-based anodes: polyacrylic acid, ACS Appl. Mater. Interfaces 2 (2010) 3004–3010.
[41] S. Hu, Z. Cai, T. Huang, H. Zhang, A. Yu, A modified natural polysaccharide as a high-performance binder for silicon anodes in lithium-ion batteries, ACS Appl. Mater. Interfaces 11 (2019) 4311–4317.
[42] C. Wang, H. Wu, Z. Chen, M.T. McDowell, Y. Cui, Z. Bao, Self-healing chemistry enables the stable operation of silicon microparticle anodes for high-energy lithium-ion batteries, Nat. Chem. 5 (2013) 1042–1048.
[43] S. Choi, T.-W. Kwon, A. Coskun, J.W. Choi, Highly elastic binders integrating polyrotaxanes for silicon microparticle anodes in lithium ion batteries, Science 357 (2017) 279–283.
[44] N. Salem, M. Lavrisa, Y. Abu-Lebdeh, Ionically-functionalized poly(thiophene) conductive polymers as binders for silicon and graphite anodes for Li-ion batteries, Energy Technol. 4 (2016) 331–340.

[45] M.T. Jeena, T. Bok, S.H. Kim, S. Park, J.-Y. Kim, S. Park, J.-H. Ryu, A siloxane-incorporated copolymer as an in situ cross-linkable binder for high performance silicon anodes in Li-ion batteries, Nanoscale 8 (2016) 9245–9253.
[46] P.-F. Cao, G. Yang, B. Li, Y. Zhang, S. Zhao, S. Zhang, A. Erwin, Z. Zhang, A. P. Sokolov, J. Nanda, T. Saito, Rational design of a multifunctional binder for high-capacity silicon-based anodes, ACS Energy Lett 4 (2019) 1171–1180.
[47] S.-M. Kim, M.H. Kim, S.Y. Choi, J.G. Lee, J. Jang, J.B. Lee, J.H. Ryu, S.S. Hwang, J.-H. Park, K. Shin, Y.G. Kim, S.M. Oh, Poly(phenanthrenequinone) as a conductive binder for nano-sized silicon negative electrodes, Energy Environ. Sci. 8 (2015) 1538–1543.
[48] M. Ling, Y. Xu, H. Zhao, X. Gu, J. Qiu, S. Li, M. Wu, X. Song, C. Yan, G. Liu, S. Zhang, Dual-functional gum Arabic binder for silicon anodes in lithium ion batteries, Nano Energy 12 (2015) 178–185.
[49] Y. Jin, B. Zhu, Z. Lu, N. Liu, J. Zhu, Challenges and recent progress in the development of Si anodes for lithium-ion battery, Adv. Energy Mater. 7 (2017), 1700715.
[50] T.M. Higgins, S.-H. Park, P.J. King, C. Zhang, N. McEvoy, N.C. Berner, D. Daly, A. Shmeliov, U. Khan, G. Duesberg, V. Nicolosi, J.N. Coleman, A commercial conducting polymer as both binder and conductive additive for silicon nanoparticle-based lithium-ion battery negative electrodes, ACS Nano 10 (2016) 3702–3713.
[51] M. Wu, X. Xiao, N. Vukmirovic, S. Xun, P.K. Das, X. Song, P. Olalde-Velasco, D. Wang, A.Z. Weber, L.W. Wang, V.S. Battaglia, W. Yang, G. Liu, Toward an ideal polymer binder design for high-capacity battery anodes, J. Am. Chem. Soc. 135 (2013) 12048–12056.
[52] H. Zhao, Y. Wei, R. Qiao, C. Zhu, Z. Zheng, M. Ling, Z. Jia, Y. Bai, Y. Fu, J. Lei, X. Song, V.S. Battaglia, W. Yang, P.B. Messersmith, G. Liu, Conductive polymer binder for high-tap-density nanosilicon material for lithium-ion battery negative electrode application, Nano Lett. 15 (2015) 7927–7932.
[53] S.J. Park, H. Zhao, G. Ai, C. Wang, X. Song, N. Yuca, V.S. Battaglia, W. Yang, G. Liu, Side-chain conducting and phase-separated polymeric binders for high-performance silicon anodes in lithium-ion batteries, J. Am. Chem. Soc. 137 (2015) 2565–2571.
[54] M.-S. Song, G. Chang, D.-W. Jung, M.-S. Kwon, P. Li, J.-H. Ku, J.-M. Choi, K. Zhang, G.-R. Yi, Y. Cui, J.H. Park, Strategy for boosting Li-ion current in silicon nanoparticles, ACS Energy Lett 3 (2018) 2252–2258.
[55] Z. Li, J. Ji, Q. Wu, D. Wei, S. Li, T. Liu, Y. He, Z. Lin, M. Ling, C. Liang, A new battery process technology inspired by partially carbonized polymer binders, Nano Energy 67 (2020), 104234.
[56] W.L. Jorgensen, D.S. Maxwell, J. Tirado-Rives, Development and testing of the OPLS all-atom force field on conformational energetics and properties of organic liquids, J. Am. Chem. Soc. 118 (1996) 11225–11236.
[57] F.S. Emami, V. Puddu, R.J. Berry, V. Varshney, S.V. Patwardhan, C.C. Perry, H. Heinz, Force field and a surface Model database for silica to simulate interfacial properties in atomic resolution, Chem. Mater. 26 (2014) 2647–2658.
[58] Z. Man, P. Li, D. Zhou, R. Zang, S. Wang, P. Li, S. Liu, X. Li, Y. Wu, X. Liang, G. Wang, High-performance lithium–organic batteries by achieving 16 lithium storage in poly(imine-anthraquinone), J. Mater. Chem. A 7 (2019) 2368–2375.
[59] B. Wang, J. Ryu, S. Choi, X. Zhang, D. Pribat, X. Li, L. Zhi, S. Park, R.S. Ruoff, Ultrafast-charging silicon-based coral-like network anodes for lithium-ion batteries with high energy and power densities, ACS Nano 13 (2019) 2307–2315.
[60] S. Kang, K. Yang, S.R. White, N.R. Sottos, Silicon composite electrodes with dynamic ionic bonding, Adv. Energy Mater. 7 (2017), 1700045.
[61] D. Liu, Y. Zhao, R. Tan, L.-L. Tian, Y. Liu, H. Chen, F. Pan, Novel conductive binder for high-performance silicon anodes in lithium ion batteries, Nano Energy 36 (2017) 206–212.
[62] W. Zeng, L. Wang, X. Peng, T. Liu, Y. Jiang, F. Qin, L. Hu, P.K. Chu, K. Huo, Y. Zhou, Enhanced ion conductivity in conducting polymer binder for high-performance silicon anodes in advanced lithium-ion batteries, Adv. Energy Mater. (2018), 1702314.
[63] L. Yue, S. Wang, X. Zhao, L. Zhang, Nano-silicon composites using poly(3,4-ethylenedioxythiophene):poly(styrenesulfonate) as elastic polymermatrix and carbon source for lithium-ion battery anode, J. Mater. Chem. 22 (2012) 1094–1099.
[64] Y. Li, K. Yan, H.-W. Lee, Z. Lu, N. Liu, Y. Cui, Growth of conformal graphene cages on micrometre-sized silicon particles as stable battery anodes, Nat. Energy 1 (2016) 15029.
[65] S. Gao, D. Yang, Y. Pan, L. Geng, S. Li, X. Li, P.-F. Cao, H. Yang, From natural material to high-performance silicon based anode: towards cost-efficient silicon based electrodes in high-performance Li-ion batteries, Electrochim. Acta 327 (2019), 135058.
[66] T.-w. Kwon, Y.K. Jeong, I. Lee, T.-S. Kim, J.W. Choi, A. Coskun, Systematic molecular-level design of binders incorporating meldrum's acid for silicon anodes in lithium rechargeable batteries, Adv. Mater. 26 (2014) 7979.
[67] J. Song, M. Zhou, R. Yi, T. Xu, M.L. Gordin, D. Tang, Z. Yu, M. Regula, D. Wang, Interpenetrated gel polymer binder for high-performance silicon anodes in lithium-ion batteries, Adv. Funct. Mater. 24 (2014) 5904–5910.
[68] B. Koo, H. Kim, Y. Cho, K.T. Lee, N.-S. Choi, J. Cho, A highly cross-linked polymeric binder for high-performance silicon negative electrodes in lithium ion batteries, Angew. Chem. Int. Ed. 51 (2012) 8762–8767.
[69] M.-H. Ryou, J. Kim, I. Lee, S. Kim, Y.K. Jeong, S. Hong, J.H. Ryu, T.-S. Kim, J.-K. Park, H. Lee, J.W. Choi, Mussel-Inspired adhesive binders for high-performance silicon nanoparticle anodes in lithium-ion batteries, Adv. Mater. 25 (2013) 1571–1576.
[70] X. Zhou, Y.-X. Yin, L.-J. Wan, Y.-G. Guo, Self-assembled nanocomposite of silicon nanoparticles encapsulated in graphene through electrostatic attraction for lithium-ion batteries, Adv. Energy Mater. 2 (2012) 1086–1090.
[71] M.J. Minch, An introduction to hydrogen bonding (Jeffrey, george A.), J. Chem. Educ. 76 (1999) 759.
[72] B.R. Bickmore, M.F. Hochella JR., D. Bosbach, L. Charlet, Methods for performing atomic force microscopy imaging of clay minerals in aqueous solutions, Clay Clay Miner. 47 (1999) 573–581.
[73] L. Wei, C. Chen, Z. Hou, H. Wei, Poly (acrylic acid sodium) grafted carboxymethyl cellulose as a high performance polymer binder for silicon anode in lithium ion batteries, Sci. Rep. 6 (2016) 19583.

Shilun Gao is a Ph. D. student under the supervision of Prof. Huabin Yang at the School of Materials Science and Engineering, Nankai University. He received his master degree in the School of Materials Science and Engineering, Tianjin University of Technology under the supervision of Prof. Lianqi Zhang in 2018. His research interests focus on the inorganic materials for rechargeable lithium/sodium ion batteries, and the design and fabrication of functional polymers for energy storage applications.

Feiyuan Sun obtained her B.Eng from HeFei University of Technology in 2018, and now is a postgraduate in the lab of Prof. Huabin Yang at the School of Materials Science and Engineering, Nankai University to pursue a Master's Degree. She works on the inorganic materials in lithium ion batteries.

Alexander Brady is a Postdoctoral Researcher at Oak Ridge National Laboratory, supervised by Andrew Stack. He received his bachelor's degree in Electrical Engineering from Cornell University. He is a materials scientist who received his PhD from Stony Brook University in 2018 (supervised by Esther Takeuchi). His research combines x-ray and neutron diffraction with advanced structure and chemical modelling techniques to understand atomic-level structure and chemical properties.

Yiyang Pan is a master student under the supervision of Prof. Huabin Yang in the School of Materials Science and Engineering, Nankai University. He received his bachelor degree in the School of Chemistry at Nankai University in 2017. His research interests focus on the polymeric materials for rechargeable lithium ion batteries.

Dandan Yang is a lab assistant at the School of Materials Science and Engineering, Nankai University. She received her bachelor degree in College of Materials Science and Technology, Beijing Forestry University in 2015, and master degree in School of Materials Science and Engineering, Nankai University in 2018. She joined Nankai University as a lab assistant in 2018. Her current research interests focus on the polymeric materials for rechargeable lithium batteries.

Vladimir Tsukruk is a Regents Professor at the School of Materials Science and Engineering, Georgia Institute of Technology. He received MS in physics from the *National University of Ukraine*, PhD, DSc degrees from the *National Academy of Sciences of Ukraine*. He serves on the *Editorial Advisory Boards* of five journals and as an Executive Editor at *ACS Applied Materials and Interfaces*. He has co-authored about 500 articles and five books. His research on synthetic and natural polymers has been recognized by Fulbright Award, Humboldt Research Award, NSF Special Creativity Award, among others. He is an elected Fellow of *APS, MRS, and ACS*.

Andrew G. Stack is a Senior R&D Staff Member at Oak Ridge National Laboratory, the Leader of the Geochemistry and Interfacial Sciences Group and Acting Director of the Chemical Sciences Division. His research interests are to understand the structure, dynamics and reactivity of aqueous solutions and mineral-water interfaces, particularly the mechanisms and kinetics of reactions such as crystal growth, nucleation and adsorption/incorporation. Typical approaches used to study these phenomena are atomic-scale simulation, X-ray/neutron scattering and scanning probe microscopies. He has authored more than 60 publications.

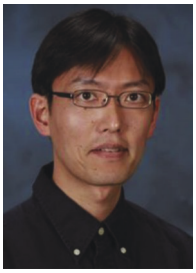

Tomonori Saito is a R&D staff scientist at Oak Ridge National Laboratory (ORNL), and a joint faculty associate professor in the Bredesen Center for Interdisciplinary Research and Graduate Education at the University of Tennessee, Knoxville. He obtained his Ph.D. in Organic Polymer Chemistry at Virginia Tech in 2008. His current projects at ORNL include polymer upcycling, self-healing polymers, thermal insulation materials for buildings, novel membranes for flow batteries, ion-conducting polymers for Li-ion and Na-ion batteries and battery binders, CO_2 separation membranes, binder development for binder jet additive manufacturing, polymeric nanoparticles, polymer nanocomposites, elastomers, and block/graft copolymers.

Huabin Yang is a professor of material science and engineering at Nankai University with expert in nanomaterials for energy storage and materials electrochemistry in high-energy batteries. Huabin Yang received his Bachelor (1993) and Doctor Degree (1998) in Physical Chemistry at Nankai University. He joined Nankai University as a research fellow in 1998 and was promoted to associate professor (2000). He moved to the National Institute of Advanced Industrial Science and Technology (Japan) as a postdoc fellow from 2002 to 2004. He returned to Nankai University (2004) and became a full professor in 2008.

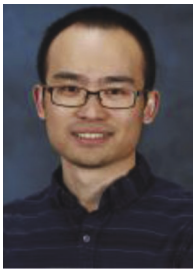

Pengfei Cao is a Staff Scientist at Oak Ridge National Laboratory (ORNL) with expert in the synthetic polymeric materials with controlled architectures and properties for both fundamental studies and application investigation. Pengfei Cao received his Bachelor and Master Degree in Chemistry at Tianjin University. After his PhD in Macromolecular Science and Engineering at Case Western Reserve University, Pengfei Cao moved to ORNL as a Research Associate in 2016, and became a R&D staff member in 2019. His current research interests are high-performance elastomers and synthetic polymers for battery applications.